

Digital Elevation Models – From Satellite Images to Free Available DEMs

Karsten Jacobsen ¹

¹ Institute of Photogrammetry and GeoInformation, Leibniz Universität Hannover, Germany - jacobsen@ipi.uni-hannover.de

Keywords: DEMs, DTMs, free available DEMs, filtering, Land Cover Map.

Abstract

Digital elevation models are an important component of any Geo-Information System (GIS). This keynote provides an overview of the satellite stereo model orientation and image matching methods currently used to generate Digital Elevation Models (DEMs). Using very high resolution stereo pairs of satellite images, DEMs with a standard height deviation in the range of 1m or even better can be generated within a limited time. Their generation is expensive, so we should have a look to free of charge available DEMs. With ASTER GDEM3, SRTM, AW3D30 and TDX-EDEM we have four global or nearly global free available. Their advantages and disadvantages are discussed. The edited version of TanDEM-X (TDX-EDEM) is the latest product published end of 2023. As reference for the analysis, LiDAR Digital Terrain Models (DTMs) with the height of the bare ground are used with an accuracy of ~ 20cm. The global or nearly global DEMs are Digital Surface Models (DSMs) with the height of the visible surface. For the comparison with the reference DTM, areas with high vegetation and buildings must be excluded, which was possible with the Land Cover Map (LCM) of TDX-EDEM. TDX-EDEM clearly offers the highest accuracy, but in steep mountains and built-up areas we should also take a look to AW3D30.

1. Introduction

Digital Elevation Models are a basic content for any Geo-Information System (GIS). The former method of ground surveying was replaced by aerial photogrammetry, which is still use, but only with automatic image matching. LiDAR is used in some countries. With LiDAR a high accuracy is reached and we have better possibilities to generate Digital Terrain Models (DTMs) with height of the bare ground. Nevertheless, LiDAR is expensive, limiting the number of countries using it as basic information. With the advent of satellites, global coverage by optical and Synthetic Aperture Radar (SAR) images came. With SPOT-1 we had the possibility to change the view direction, required for stereoscopic imaging, but with the disadvantage of time delay of the second image of the stereo pair. With the flexible satellites, the difference in time difference between the two images of a stereo pair could be reduced to less than 90 seconds. However, for a global stereoscopic coverage stereo satellites with 2 or even 3 cameras are required, leading to a nearly global coverage by ASTER and later with higher resolution by the stereo camera of ALOS. Optical images require sunlight and a cloud free coverage. This is not the case for SAR, radar can penetrate clouds and it is an active system not requiring sunlight. For a global coverage, Interferometric SAR (InSAR) (Ferretti et al. 2007) is required with 2 antennas. With the Shuttle Radar Topography Mission (SRTM) this was the case in year 2000. With better resolution and multiple coverage an improvement came with the TanDEM-X satellite mission starting in 2013.

The used DEMs have been analysed before e.g. (Wessel et al. 2018), (Tadono et al. 2014), (Rodriguez et al. 2005) and (Abrams et al. 2022), but their investigations were limited to the absolute accuracy of the DEMs, no qualified reference DEM was used and the analysed DEMs had to be compared in the same area. Furthermore, the edited version of TanDEM-X (TDX-EDEM), available since the end of 2023 has not been intensively investigated. The global and nearly global DEMs are Digital Surface Models (DSMs) with the height of the visible surface, while the used LiDAR reference DEMs are Digital Terrain Models (DTMs) with the height of the bare ground. The parts influenced by high vegetation and buildings had to be removed

from the analysis, and this is now easily possible with the TDX-EDEM Land Cover Map (LCM).

2. DEM with Satellite Images

2.1 Image Orientation of Optical Images

With the exception of some small size satellites, current optical satellites are push broom imagers that record one line after the other with satellite movement and changes of the view direction. Originally, the orientation is determined by geometric reconstruction, but this is individual for any satellite, so the replacement model Rational Polynomial Coefficients (RPC) is common, and usually is distributed together with the satellite images (Jacobsen et al. 2005). The accuracy of the RPC can be improved by using Ground Control Points (GCP), usually through an affine transformation as bias corrected RPC, nevertheless, often a simple shift is satisfying. Not in any case RPC are available, and without knowledge of imaging details, approximate solutions as the 3D-Affine Transformation can be used.

The common formula for 3D-Affine Transformation is (1).

$$\begin{aligned}x_{ij} &= a_1 + a_2 * X + a_3 * Y + a_4 * Z \\y_{ij} &= a_5 + a_6 * X + a_7 * Y + a_8 * Z\end{aligned}\quad (1)$$

where x_{ij} and y_{ij} are the image coordinates,
 X, Y, Z = ground coordinates

This formula (Hanley et al. 2002) represents an approximation that is satisfactory for flat areas, but for larger height differences, it has to be extended to (2).

$$\begin{aligned}x_{ij} &= a_1 + a_2 * X + a_3 * Y + a_4 * Z + a_9 * X * Z + a_{10} * Y * Z \\y_{ij} &= a_5 + a_6 * X + a_7 * Y + a_8 * Z + a_{11} * X * Z + a_{12} * Y * Z\end{aligned}\quad (2)$$

(Büyüksalih et al. 2008).

With satisfying GCP a standard deviation below one Ground Sampling Distance (GSD) can be reached (Jacobsen et al. 2005).

2.2 Digital Elevation Models by Optical Satellite Images

The vertical accuracy of image orientation in case of stereo models depends slightly on the base to height relation (Figure 1). Under optimal condition a standard deviation of the height (SZ) of 1 GSD can be reached (Büyüksalih, Jacobsen, 2006) (Figure 1).

$$SZ = h/b * Sp_x \quad (3)$$

Vertical accuracy as function of height to base relation.

For images taken in nadir direction, we have the relation (3) between the standard deviation of the x-parallax (Sp_x) and the standard deviation of the height (SZ). This formula comes from aerial images, where the parallax px is the difference between the x-image coordinates. For satellite stereo pairs, we have a convergent viewing direction, but due to the small field of view of satellite images, formula 3 can also be used for satellite images if the image coordinates in base direction are divided by the cosine of half the angle of convergence, which has a limited influence. However, for automatic image matching Sp_x depends on angle of convergence. When the angle of convergence is small, the images are more similar, leading to more accurate matching, as in case with a larger angle of convergence, as shown in Figure 1. Formula 3 only gives the correct relationship for flat areas. A smaller convergence angle should be used, especially in built-up areas.

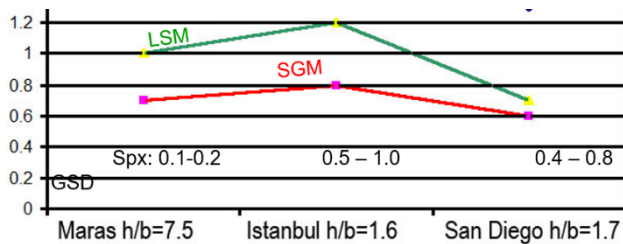


Figure 1. Standard deviation of building height determination in the center as function of height to base relation [GSD] by least squares matching (LSM) and semi global matching (SGM).

The images used for the DEM generation should come from the same orbit with forward up to backward view direction. This guarantees the same object situation. A stereo view from different orbits, as it was the case for the first SPOT satellites, may cause problems for image matching due to changes in the object. DEMs are generated by area based or feature based automatic image matching. The classical image correlation commonly was replaced by least squares matching, SIFT or SURF, Dynamic Programming, Semi Global Matching and several sub-versions. Semi Global Matching has advantages in built-up areas (Alobeid et al. 2010) for sharp definition of buildings (Figure 2), but SIFT and SURF are more robust in countryside.

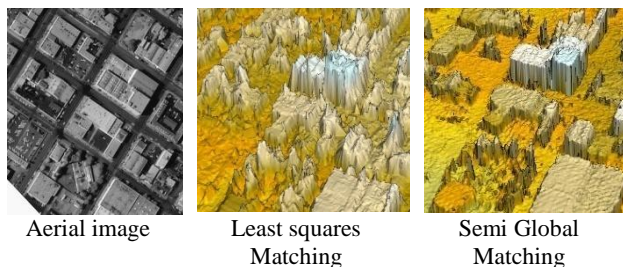


Figure 2. DSM generated by least squares matching and by semi global matching in relation to aerial image (Alobeid et al. 2010).

Beside the method of image matching, the accuracy of DEMs strongly depends on the terrain inclination.

$$SZ = A + B * \text{tangent (slope)} \quad (4)$$

where A and B are the coefficients describing SZ.

With optical images, Digital Surface Models (DSMs) are generated with the height of the visible surface, while often DTMs are requested. If there are isolated buildings and trees in the object area, these objects can be eliminated by filtering (Passini et al. 2002). This is not possible for larger forest areas and dense built-up areas. When determining water depth in shallow waters, avoid looking towards the sun, as this may result in total reflections. Two views opposite to the sun, one with lower and one with higher nadir angle, should be preferred.

2.3 Synthetic Aperture Radar

The handling of SAR is described in (Ferretti et al. 2007 and Sefercik et al. 2018) in detail. Radar has the advantage that it can penetrate clouds and is independent on sunlight. Cloud free condition is a bottleneck for optical images. On the other hand, Radar has disadvantages in steep mountains and build-up areas due to Radar layover and larger Radar shadows as by optical images. With Sentinel-1 free C-band Radar images are available and together with the free software of ESA anybody can generate the own actual DEMs. C- and X-band Radar cannot penetrate the vegetation, this is just possible with the longer L-band. Currently no free L-band images are available, but this may change.

In areas with steep slopes, Radar has the disadvantage of layover, foreshortening and larger shadows (Figure 3). For this reason in steep mountainous and in built-up areas, Radar imaging has some disadvantages against optical images. On the other hand, Radar images have less problems with the accuracy of direct sensor orientation as optical images, their ground location depend on the more precise distances from the satellites.

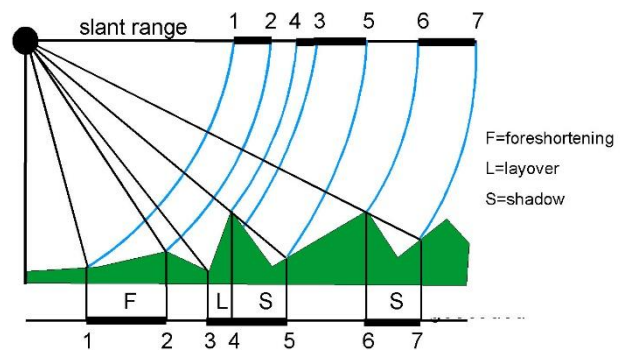


Figure 3. Problems of Radar images.

3. Digital Terrain Models

3.1 General

RM SE	SZ	NMAD	Median	LE90	LE95
Root mean square	Standard deviation	Normalized median absolute deviation	50% probability	Linear error 90% probability	Linear error 95% probability

Table 1. Accuracy figures for DEMs.

For DEMs the accuracy figures in Table 1 are in use. The root mean square error (RMSE) is based on the original discrepancies of the DEM against the reference DEM, while for the standard deviation of Z (SZ) the bias (shift in Z) is split of. The Normalized Median Absolute Deviation (NMAD) (Höhle and Höhle 2009) is based on the median, which has a probability of 50%. For normalizing it to the probability level of SZ, NMAD is the median multiplied with 1.4826 to be identical to SZ with a probability of 68.27% under condition of exact normal distribution of the differences. Typically, we have more larger discrepancies than corresponding to the normal distribution, resulting in a larger value for SZ than for NMAD. LE90 and LE95 are not accuracy numbers, but tolerance limits and do not describe the accuracy.

Although free satellite images are available, in most cases GCP are required and in addition, it is time consuming to generate DEMs. Global or nearly global DEMs are available free of charge and it should be checked if these DEMs are satisfying for the required purposes. The investigation is limited to ASTER GDEM version 3, SRTM, AW3D30 and TDX-EDEM. There are more global or nearly global DEMs, but they cannot compete with these and therefore not included. For example, TDM90 is not included in in this investigation and following analysis, it is replaced by TDX-EDEM.

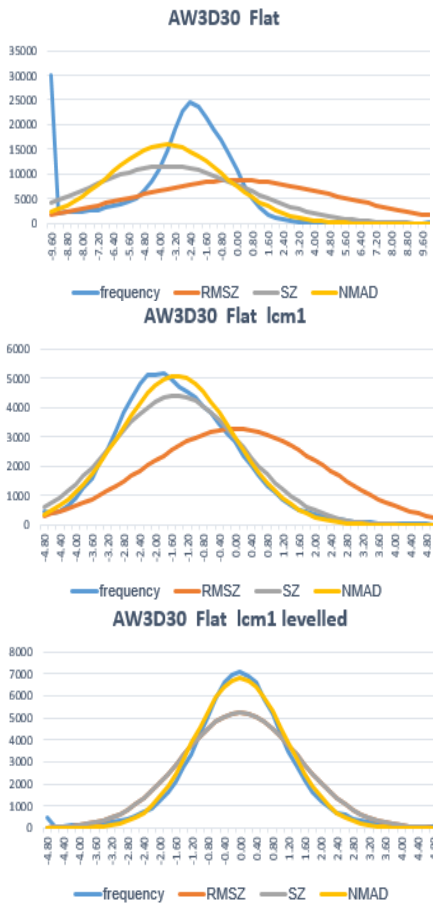


Figure 4. Frequency distribution of AW3D30, test site Flat blue=frequency distribution, normal distributions based on RMSZ=brown, SZ = grey, NMAD=yellow.

If the whole DEM is analysed, a higher number of large differences appear and the normal distributions based on RMSZ, SZ and NMAD do not fit to the frequency distribution (Figure 4, upper). If the analysis is limited to the open area, using LCM as area for exclusion, the normal distribution based on SZ and NMAD fit better to the frequency distribution (Figure 4, centre). If the systematic errors caused by the tilt of the DEM are respected by levelling (see also Figure 6), the normal distribution based on NMAD fits very well to the frequency distribution (Figure 4, lower), nevertheless the normal distribution based on RMSZ and SZ are not fitting as well. For this reason, NMAD describes the accuracy better as SZ. This is not limited to the data set used, but is typical.

Whole DEM, original differences

Range +/- 9.6m

Only open area

Range +/- 4.8 m

Only open area after levelling of DEM

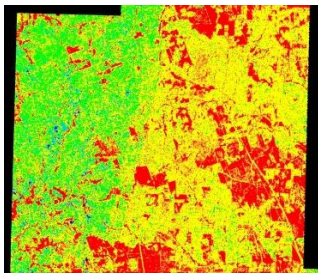
	GDEM3	SRTM	AW3D30	TDX-EDEM
organization	NGA, NASA	METI, NASA	JAXA	DLR
source	Optical ASTER 15m GSD	Shuttle InSAR	Optical ALOS PRISM 2.5m GSD	Edited TanDEM-X InSAR + LCM
Latitude	+/- 83°	56° S – 60° N	+/- 82°	global
acquisition	2000 - 2011	11 days in 2000	2006 - 2011	2013 - 2016

Table 2. Free available DEMs.

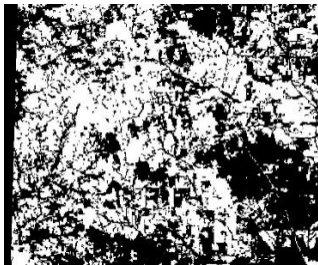
All DEMs listed in Table 2 have a point spacing of 1 arcsecond, corresponding to 30.86 m at the equator and due to the convergence of meridian and the location of the test sites at approximately 31° North to a spacing in east-west direction to 26.5 m or in the average approximately to 29m. The DEMs were verified with a LiDAR reference with a point spacing of 2.5 m and a vertical standard deviation (SZ) of approximately 0.2 m. Four test sites were used to cover the main different types of areas: Mountain, located in Arizona with steep mountains and no vegetation and buildings; Rolling, as the other test sites located in Texas, Flat and City with larger percentage of built-up areas. The DEM-points do not have exactly the same location as the reference DEM, requiring an interpolation. The influence of a bilinear interpolation to the point spacing of the reference was investigated. If the reference DEM has a point spacing of 30 m instead of 2.5 m, in the test sites Rolling, Flat and City, there is an influence to the root mean square Z-differences of 15 cm up to 37 cm, but in the rough mountainous area the loss of accuracy is 3.02 m. For this reason, the reference with a spacing of 2.5 m was used.

3.2 Analysis of the Free DEMs

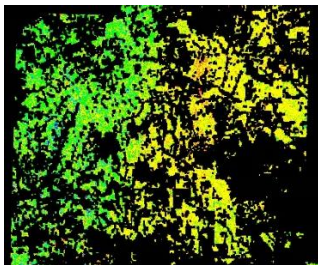
Since vegetation cannot be penetrated by optical rays and radar C- and X-band, DEMs are generated as digital surface models with the height of the visible surface, but usually digital elevation models with the height of the bare ground are requested. If only single trees and single buildings are available, these can be filtered out (Passini et al, 2002). However, very often larger areas are covered by forest, and if no height information of the bare ground is available, interpolation to the neighbored ground points can lead to errors. The reference LiDAR DEM is a DTM and this cannot be directly be compared with a DSM. TDX-EDEM comes together with a Land Cover Map (LCM). This LCM can be used as a layer to exclude parts with higher vegetation and buildings from the analysis. Especially in SAR DEMs, layover and shadows can affect the area near the LCM, for this reason and based on the results obtained, the LCM was extended by 1 pixel towards the area outside the LCM.



Colour coded Z-differences of AW3D30



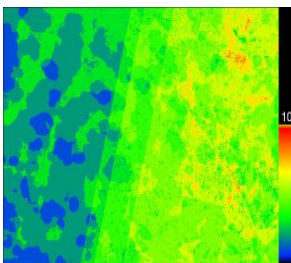
Land cover map (LCM)



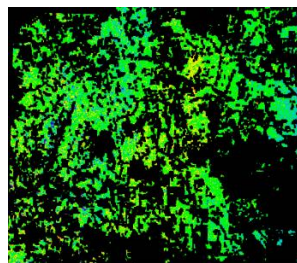
Colour coded Z-differences of AW3D30 in the open area

Figure 5. Influence of high vegetation and buildings in test site Flat, colour scale: < 6 m = red, >6 m = violet.

Figure 5 upper shows the colour coded height differences for AW3D30 against the reference DTM in test site Flat. The red parts are caused by high vegetation and buildings, which are mainly influenced by elements not belonging to a DTM. Figure 5, centre, shows the LCM extended by 1 pixel, fitting very well with the with the red parts on left hand side. Figure 5 lower shows the colour coded height differences of AW3D30 against the reference using a layer of exclusion based on LCM. In this case, no red pixels indicating large height differences are included. Figure 5, right, shows on right side yellow pixels presenting height differences between -1.2 m and -2.4 m, indicating a tilt of the DTM which was adjusted to -3.5 m over 17 km in East-West direction. Such systematic errors can be eliminated by levelling in relation to the reference DEM (Figure 6 right), but even with a not so precise DEM. A reason for the DEM tilt is the combination of up to 10 original AW3D30 DEMs (Figure 6 left).



Number of original AW3D30 DEM coverages



Colour coded Z-differences of AW3D30 after levelling

Figure 6. Reason for tilt and improvement of DEM – AW3D30 in test site Flat.

Systematic differences in height also can be caused by a shift of the DEM in X and Y. For this reason, at first the horizontal shifts

have been determined with Hannover DEMSHIFT program. Significant horizontal shifts were only found for ASTER GDEM3 and AW3D30 in test site Mountain.

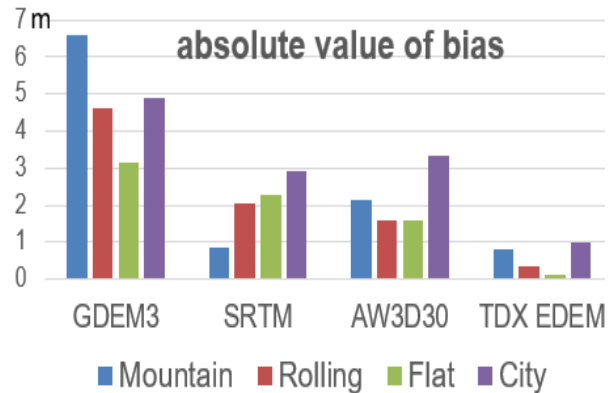


Figure 7. Bias of the DEMs in the used test sites.

The bias (systematic height shift) of the ASTER GDEM3 DEMs is significantly than for the other 3 DEM types. TDX-EDEM has the best absolute orientation in all test sites with bias below 1.0 m. The other DEMs could be improved by reference DEMs, whose standard deviation does not have to be smaller due to the high number of points in the DEMs.

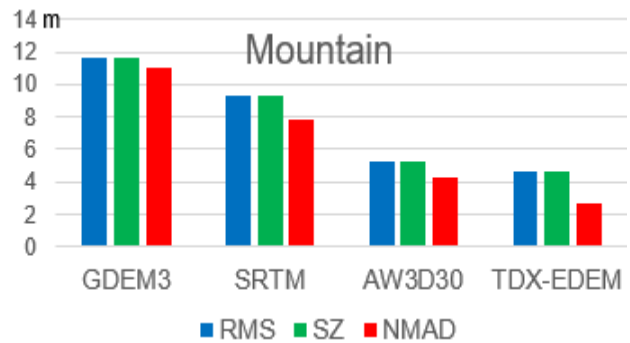


Figure 8. Accuracy of DEMs in test site Mountain.

	GDEM3	SRTM	AW3D30	EDEM
NMAD	11.20	7.92	4.59	2.82
NMAD F(slope)	6.81 + 19.4*tan α	4.00 + 16.9* tan α	1.73 + 10.6* tan α	1.34 + 5.2 tan α
NMAD <0.1 (5.7°)	6.37	3.75	1.29	1.69

Table 3. NMAD, NMAD as function of slope, NMAD for points with slope < 5.7°, test site Mountain, unit = [m].

In test site Mountain the analysed DTMs are DSMs due to missing vegetation and buildings, requiring no layer for exclusion. The overall NMAD (Table 3, 1st line) shows clear differences in accuracy corresponding to the sequence of the DSMs in Table 3. The NMAD as function of slope shows the same sequence. The NMAD for points with a slope < 5.7° shows a better NMAD for AW3D30 than for TDX-EDEM. This may be caused by an influence of Radar layover for TDX-EDEM, which is not present for optical images used for AW3D30.

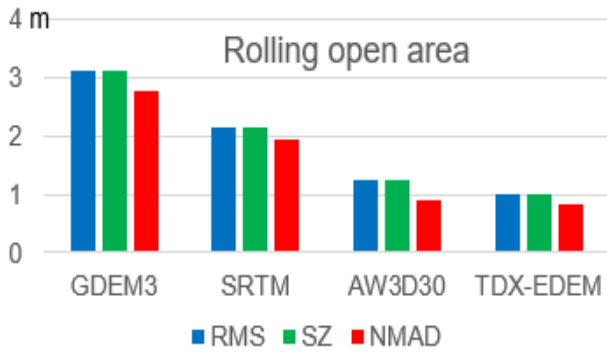


Figure 9. Accuracy of DEMs in open area of test site Rolling.

	GDEM3	SRTM	AW3D30	EDEM
NMAD	2.80	1.95	0.90	0.87
NMAD F(slope)	2.70 + 5.5*tan α	2.10 + 1.3*tan α	0.90	0.59 + 2.9*tan α
NMAD <0.1 (5.7°)	2.66	1.92	0.88	0.70

Table 4. NMAD, NMAD as function of slope, NMAD for points with slope < 5.7°, test site Rolling, unit = [m].

Figure 9 looks similar to Figure 8 at first glance, but the scale is quite different due to missing very steep parts in test site Rolling. In test site Rolling, NMAD in TDX-EDEM is slightly better as for AW3D30. Nevertheless, in both test sites the absolute accuracy (RMSE) for TDX-EDEM is better as for AW3D30 (Figures 8 and 9).



Figure 10. Accuracy of DEMs in open area of test site Flat.

	GDEM3	SRTM	AW3D30	EDEM
NMAD	3.44	2.39	1.50	0.57
NMAD F(slope)	3.19 + 0.7*tan α	2.88 + 0.5*tan α	1.50	0.52 + 0.5*tan α
NMAD <0.1 (5.7°)	3.44	2.35	1.48	0.53

Table 5. NMAD, NMAD as function of slope, NMAD for points with slope < 5.7°, test site Flat, unit = [m].

In test site Flat, NMAD for TDX-EDEM is significantly better than for AW3D30. The absolute orientation of the AW3D30 DEM is also not as good as for TDX-EDEM.

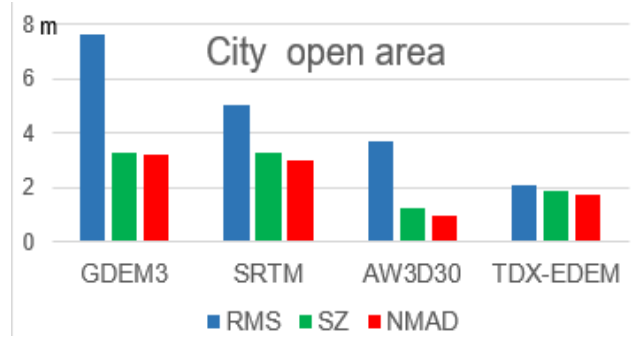


Figure 11. Accuracy of DEMs in open area of test site City.

	GDEM3	SRTM	AW3D30	EDEM
NMAD	3.22	2.98	0.95	1.75
bias	-6.85	-3.79	-3.45	-0.91
NMAD <0.1 (5.7°)	1.80	2.69	0.95	1.59

Table 6. NMAD, NMAD as function of slope, NMAD for points with slope < 5.7°, test site City, unit = [m].

The test site City shows large differences between RMSE and SZ, caused by the large bias (Figure 11, Table 6). With the exception of EDEM, the bias is strongly influenced by the built-up area. In the test site City, no dependency on the tangent of the slope could be determined.

All four sites show the lowest accuracy for ASTER GDEM3, followed by SRTM, therefore ASTER GDEM3 and SRTM elevation models should no longer be used. The decision for TDX-EDEM and AW3D30 is more complex. TDX-EDEM has a better orientation, with a smaller bias and no DEM tilt. The absolute accuracy for TDX-EDEM is better than that of AW3D30. However, if a reference DEM, even with a lower accuracy, can be used for an improvement, AW3D30 may offer some advantages in steep mountainous areas and built up areas due to layover effects of the SAR. Nevertheless, in general TDX-EDEM has some advantages.

A check of the contour lines in test site Mountain showed approximately the same quality of the contour lines based on TDX-EDEM and AW3D30 in relation to the LiDAR reference. The contour lines based on SRTM and ASTER GDEM were not as good.

4. Conclusion

The generation of DEMs from satellite images with orientation by RPC is standard since some years. The orientation by the approximation of 3D-affine orientation is possible for limited height differences. For larger height differences in the stereo model, the extended formula 2 should be used. For the DEM determined by image matching, the height-to-base ratio is not so important; especially in build-up areas, a smaller angle of convergence has advantages.

The free DEMs ASTER GDEM3, SRTM, AW3D30 and TDX-EDEM have been analysed. ASTER GDEM3 is based on the optical ASTER images with 15m GSD, while AW3D30 is based on the optical ALOS images with 2.5 m, so it is not a surprise, that the ASTER GDEM3 images cannot reach the accuracy of AW3D30. SRTM uses C-band SAR images, taken during 11 days in 2000 from the Space Shuttle. Only few scenes have been determined twice. TanDEM-X (SAR X-band) used better scene combinations, a higher resolution and more scenes covering the same area, and was also enhanced by post-processing, leading to better results as SRTM. The previously widely used SRTM DEM

should be replaced by TDX-EDEM, just as ASTER GDEM3 should be replaced by AW3D30. In general, TanDEM-X has a better geo-reference than AW3D30 and in addition in most cases also a better NMAD than AW3D30. However, in steep mountainous regions and in built-up areas, AW3D30 is not affected by radar layover and may have a better relative accuracy. The TDX EDEM land cover map is usable for a layer of excluding the areas covered by high vegetation and buildings to allow an analysis limited to the DTM parts.

ISPRS Annals of the Photogrammetry, Remote Sensing Spatial Information Science, 2(4), 71.

Wessel, B., Huber, M., Wohlfart, C., Marschalk, U., Kosmann, D., Roth, A., 2018. Accuracy Assessment of the Global TanDEM-X Digital Elevation Model with GPS Data. *ISPRS Journal of Photogrammetry and Remote Sensing*, 139, 171-182.

Acknowledgements

Thanks are going to NASA, METI, JAXA and DLR for the free distribution of the global or nearly global height models.

References

Abrams, M., Yamaguchi, Y., Crippen, R., 2022. ASTER global DEM (GDEM) version 3, *ISPRS Archives XLIII-B4-2022*.

Alobeid, A., Jacobsen, K., Heipke, C., 2010. Comparison of Matching Algorithms for DSM Generation in Urban Areas from IKONOS Imagery, *PERS* 76(9), 1041-1050

Büyüksalih, G., Akcin, H., Jacobsen, K., 2006. Geometry of OrbView-3 images. *ISPRS Ankara Workshop Topographic Mapping from Space, ISPRS Archives XXXVI-1/W41*.

Büyüksalih, G., Jacobsen, K., 2008. Digital Height Models in Mountainous Regions based on Space Information. *EARSeL Workshop Remote Sensing - New Challenges of High Resolution, Bochum*.

Ferretti, A., Monti-Guarnieri, A., Prati, C., Rocca, F., 2007. InSAR Principles: Guidelines for SAR Interferometry, Processing and Interpretation; ESA, https://www.esa.int/About_Us/ESA_Publications/InSAR_Principles_Guidelines_for_SAR_Interferometry_Processing_and Interpretation_br_ESA_TM-19, Access September 2024.

Hanley, H.B., Yamakawa, T., Fraser, C.S., 2002. Sensor Orientation for High Resolution Imagery, *Pecora 15 / Land Satellite Information IV / ISPRS Archives XXXIV part 1*.

Höhle, J., Höhle, M., 2009. Accuracy assessment of digital elevation models by means of robust statistical methods. *ISPRS Journal of Photogrammetry and Remote Sensing*, 64(4), 398-406.

Jacobsen, K., Büyüksalih, G., Topan, H., 2005. Geometric Models for the Orientation of High Resolution Optical Satellite Sensors, *ISPRS Archives XXXVI-1/W3*.

Passini, R., Betzner, D., Jacobsen, K., 2002. Filtering of Digital Elevation Models. *ASPRS Annual Convention*, Washington.

Rodriguez, E., Morris, C.S., Belz, J.E., 2006. A global assessment of the SRTM performance. *Photogrammetric Engineering and Remote Sensing*.

Sefercik, U., Büyüksalih, G., Atalay, C., Jacobsen, K., Karakis, S., 2018. Analysis of Sentinel-1A, AW3D30 and SRTM Digital Surface Models in Relation to Laser Scanner Reference as Function of Terrain Classes, *PFG*, 86(3–4), 141–155.

Tadono T, Ishida H., Oda F., Naito S., Minakawa K., Iwamoto H., 2014. Precise global DEM generation by ALOS PRISM.